Anisotropic high cycle fatigue behavior of Ti–6Al–4V obtained by powder bed laser fusion

Dear Author,

Please, note that changes made to the HTML content will be added to the article before publication, but are not reflected in this PDF.

Note also that this file should not be used for submitting corrections.

International Journal of Fatigue xxx (2016) xxx–xxx

Contents lists available at ScienceDirect

International Journal of Fatigue

journal homepage: www.elsevier.com/locate/ijfatigue

Anisotropic high cycle fatigue behavior of Ti–6Al–4V obtained by powder bed laser fusion

Gianni Nicoletto

Department of Industrial Engineering, University of Parma, Parco Area delle Scienze 181/A, 43124 Parma, Italy

ARTICLE INFO

Article history:
Received 16 March 2016
Received in revised form 5 April 2016
Accepted 29 April 2016
Available online xxxx

Keywords:
Fatigue
Ti–6Al–4V
Powder bed fusion
Miniature specimen
Microstructure

ABSTRACT

An original fatigue test methodology aimed at PBF materials is presented and directed to the evaluation of the anisotropic fatigue behavior of DMLS Ti6Al4V. The presence of such anisotropy is intrinsic to the specific and complex microstructure obtained by the layer-by-layer development of the part produced by DMLS. Comparison of the present test results with data obtained with a variety of test methods and test parameters clarified the role of intrinsic (material-dependent) and extrinsic (test-method-dependent) factors on the measured fatigue behavior. The proposed testing method permits substantial cost saving in terms of material and process time, benefits that are especially welcome for developmental studies of PBF alloys and process parameters.

1. Introduction

Additive Manufacturing (AM) is an innovative technological trend that will influence the future of the manufacturing industry [1]. AM technologies enable layer-by-layer fabrication of complex parts directly from CAD files without part-specific tooling [2]. Additive manufacturing offers many strategic advantages including increased design freedom for building internal and external part geometries that cannot be made in any other way and the possibility of building functional parts in small lot sizes for end-user customization [1,2]. The ability to net-shape manufacture complex parts without the need of expensive tooling and machining minimizes the delay between design and manufacture.

Powder bed fusion (PBF) technology defines a specific subset of AM technologies in which a metal powder is selectively melted layer-by-layer by a computer-driven concentrated energy beam. The most widely used heating energy of the PBF processes is a highly focused laser beam although the electron beam is alternatively used. Manufacturer-related acronyms such as Direct Metal Laser Sintering (DMLS), Selective Laser Melting (SLM) and Laser Cusing can be grouped under the PBF acronym. An advantage of the PBF technology is that only the locally melted powder transforms into a solid material while the remaining powder can be reused a number of times. All PBF systems can process powders of a relatively large range of metal alloys, such as titanium alloys, stainless steels and Ni-based alloys [1,2]. Titanium alloys are possibly the PBF materials under most intense investigation. The excellent strength and toughness, combined with the corrosion resistance, low specific weight and biocompatibility of Ti–6Al–4V, make it ideal for many high-performance engineering applications in aerospace and motor racing, but also for the production of biomedical implants, due to its higher strength, low modulus and fatigue resistance.

The PBF technologies applied to Ti–6Al–4V share a number of drawbacks: due to the typical process conditions, (i.e. layer by layer generative principle, short energy pulses resulting in highly localized melting and solidification and strong temperature gradients of this manufacturing process), the microstructure exhibits strong directionality, consequently anisotropic structure, i.e. columnar grain structure, and mechanical properties [3–8]. Residual stresses are also expected due to this process and can be managed by appropriate post-fabrication heat treatment [7,9]. This new manufacturing technique may present porosity [5]. The strongly textured microstructures results in anisotropy of the mechanical properties [8].

The PBF technology penetration in and acceptance by industry are somehow hampered by the relative slow pace of material characterization, which is a fundamental ingredient of part design and qualification. While many references, for example [4–8], discuss the link between process parameters and static mechanical properties of PBF Ti–6Al–4V, the fatigue strength characterization appears more recently in the literature [10–15], and the published results are somewhat difficult to generalize. Fatigue testing is known to be expensive and time consuming as it is susceptible

E-mail address: gianni.nicoletto@unipr.it

http://dx.doi.org/10.1016/j.ijfatigue.2016.04.032
0142-1123/

Please cite this article in press as: Nicoletto G. Anisotropic high cycle fatigue behavior of Ti–6Al–4V obtained by powder bed laser fusion. Int J Fatigue (2016), http://dx.doi.org/10.1016/j.ijfatigue.2016.04.032

to a number of intrinsic and extrinsic factors that complicates the data generalization and exploitation [15]. On the other hand, the fatigue behavior of PBF-transformed Ti–6Al–4V is critical for sectors, in which high structural integrity is a paramount requirement, i.e. aerospace and motorsport.

In this contribution an original fatigue test methodology especially aimed at PBF materials is presented and directed to the evaluation of the anisotropic fatigue behavior (i.e. dependent on direction) of Ti6Al4V obtained using the DMLS process. Structural anisotropy is intrinsic to the specific the layer-by-layer development of a part produced by DMLS, but it is a concern in view of part qualification. While the directionality of static mechanical properties of DMLS Ti6Al4V has been documented [8], little information is available of such influence on the high cycle fatigue behavior.

2. Fatigue specimen geometry and test method

Savings in material, time and money guided the development of the present test method. Flexibility of use, i.e. evaluation of surface effects, detection of damage initiation and development, were also requirements taken into consideration.

The new fatigue test method adopts a specific miniature specimen geometry. The specimen design shares the nominal cross-sectional area (5×5 mm^2) with the specimen geometry of a Schenk–Erlinger type machine, therefore a sectional modulus $W = 20.8$ mm^3. This value of the sectional modulus is practically the same of the common 6-mm-dia rotating bending geometry, i.e. $W = 21$ mm^3.

On the other hand, the material saving of the miniature specimen geometry is immediately apparent by the comparison with the standard geometry in Fig. 1. The volume of the miniature specimen is approx. 1/6 of the standard specimen. Furthermore, its max dimension is length $L = 22$ mm, see Fig. 2, compared to $L = 90$ mm of the recommended specimen geometry. These characteristics greatly simplify and reduce the costs of multiple specimen production especially in the build direction.

The new specimen design was developed to be tested in a Schenk–Erlinger cyclic plane-bending machine. It required however required the adaptation of the grips to securely hold the miniature specimens ends and apply a pure bending load. Fig. 3 shows the miniature specimen mounted in the fatigue testing machine.

The fatigue machine works in controlled end-specimen rotation mode applied to the miniature specimen at 20 Hz frequency. The applied bending load is continuously monitored throughout the test by a load cell in series with the specimen as shown Fig. 3. Fig. 4 shows an example of the evolution of the max bending load during an entire test and the definition of cycles to failure: the fatigue test is terminated when the initially applied bending load shows a 10% reduction. Therefore, the present test method yields the dependence of the number of cycles to crack initiation on the cyclic bending stress.

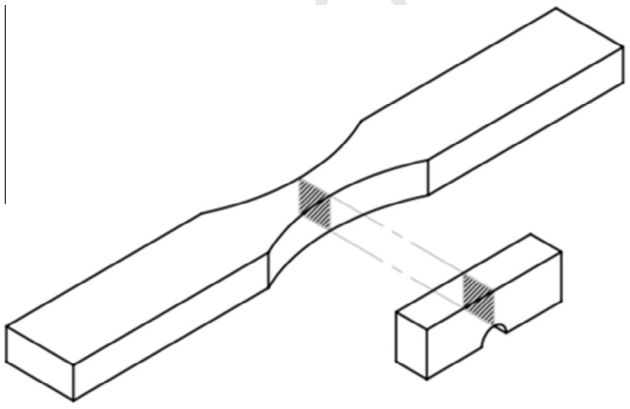

Fig. 1. Miniature specimen vs. standard specimen.

Fig. 2. Actual size ($7 \times 5 \times 22$ mm^3) of a DSLM miniature fatigue specimen.

To localize the fatigue crack initiation at the center of the smooth top surface of the plane bending specimen, the prismatic geometry ($7 \times 5 \times 22$ mm^3) presents a 2-mm-round notch on the opposite side, see Fig. 5. The bending specimen geometry was optimized using the finite element method. Fig. 5 shows the principal stress distribution due to bending within the specimen (i.e. only half specimen was modeled exploiting a geometrical symmetry). The elastic FE analysis shows also the presence of stress concentrations due to the grips, which were however minimized to favor crack initiation at the desired central location.

In the fatigue experiments, the top flat surface is subjected to tensile loading (i.e. plane bending with load ratio $R = \sigma_{min}/\sigma_{max} = 0$) while the smooth round notch in compression on the opposite surface influences crack initiation at mid length of the flat surface. Fig. 6 shows the elastic principal stress distribution in the minimum cross-section compared to the nominal bending stress distribution. It shows an almost constant stress gradient on the tensile side and a surface stress about 8% less the nominal value.

As a first approximation, the nominal stress σ due to bending is given by $\sigma = M/W$ where M is the applied bending moment and the sectional modulus $W = BH^2/6$ with B and H the width and height of the nominal specimen cross section, respectively (here $B = H = 5$ mm). When data generated with different smooth specimen geometries are available, they can be compared to the data obtained with this specimen geometry applying an effective stress factor obtained by elastic FEA as follows

$$\sigma_{eff} = 0.92\sigma \quad (1)$$

While this new fatigue testing system and specimen geometry were developed using previously characterized metallic materials, here the experimental method is applied to the fatigue testing of DMLS Ti6Al4V with the objective of quantifying the influence of the anisotropic microstructure due to the material fabrication process on the high cycle fatigue behavior. Therefore, three sets of specimens with three different orientations with respect to build, shown in Fig. 7, were conveniently manufactured and tested in plane bending under stress ratio $R = 0$ at 20 Hz loading frequency at room temperature. Tests were interrupted (i.e. run out) when specimens reached $2 \cdot 10^6$ cycles without failure.

3. Specimen production and characterization

3.1. Material production

A pre-alloyed Ti6AlV4 alloy in fine powder form with a granulometry in the 24–53 μm diameter range was processed in an

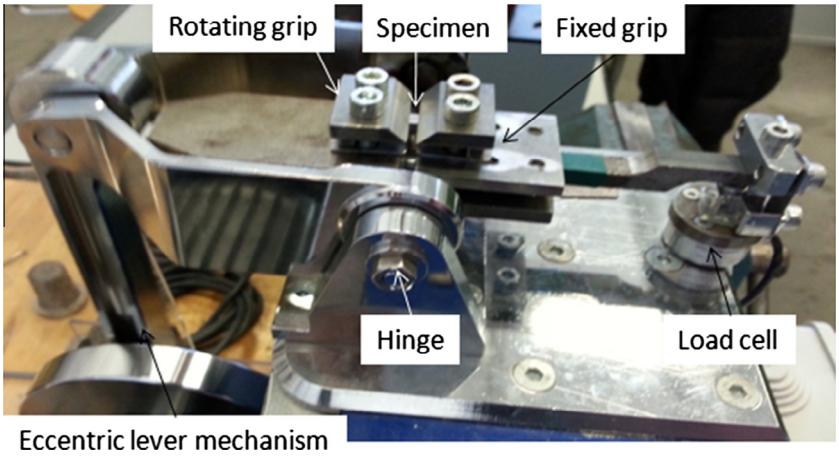

Fig. 3. Miniature specimen mounted in the Schenk–Erlinger-type testing machine.

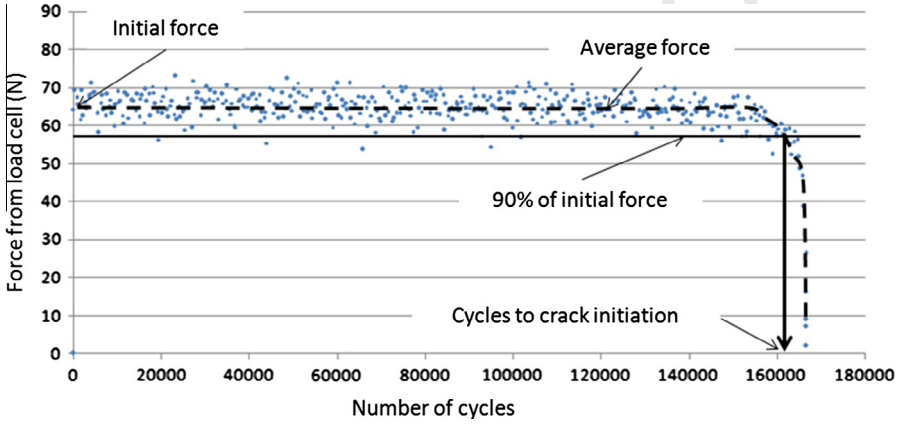

Fig. 4. Evolution of bending force measured by the load cell during a test and definition of test end.

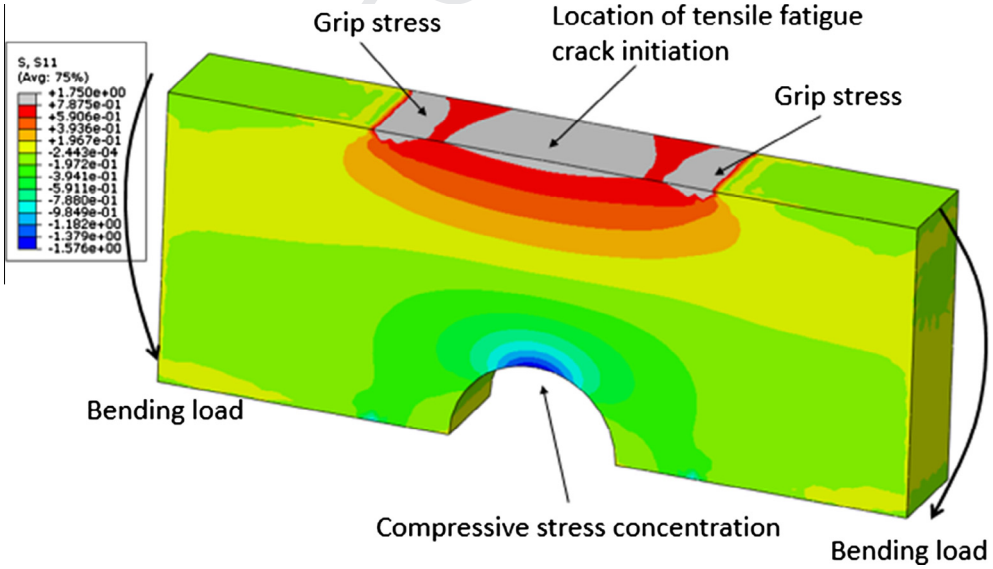

Fig. 5. Principal stress distribution due to bending in half-thickness miniature specimen.

EOSINT M270 system (EOS GmbH, Germany) according to optimized process parameters. The maximum build volume of the system is 250 mm × 250 mm × 215 mm. EOS implements the Direct Metal Laser Sintering (DMLS) process using Ytterbium fiber laser (wavelength of 1075 nm) and a power of 200 W. The focused beam selectively melts a powder layer of approx. 30 μm in thickness.

After the specimen fabrication phase, a heat treatment (380 °C for 8 h in vacuum followed by cooling in Argon atmosphere) was

Please cite this article in press as: Nicoletto G. Anisotropic high cycle fatigue behavior of Ti–6Al–4V obtained by powder bed laser fusion. Int J Fatigue (2016), http://dx.doi.org/10.1016/j.ijfatigue.2016.04.032

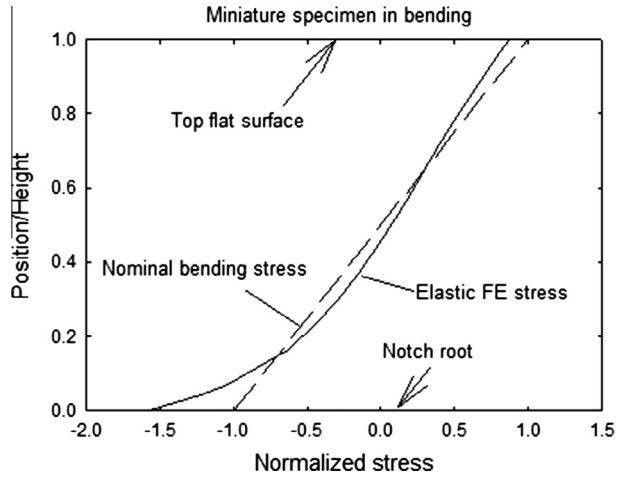

Fig. 6. Principal stress distribution due to bending in half miniature specimen.

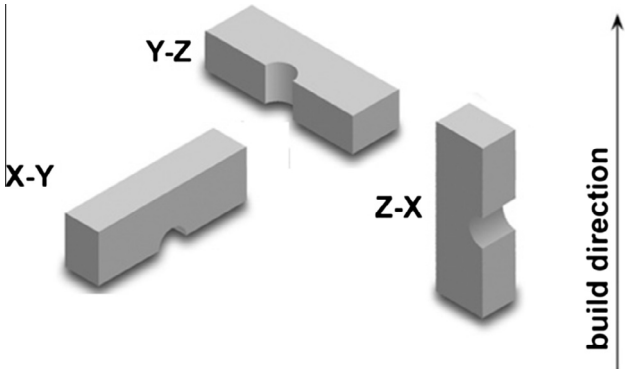

Fig. 7. Miniature specimen orientations with respect to build direction.

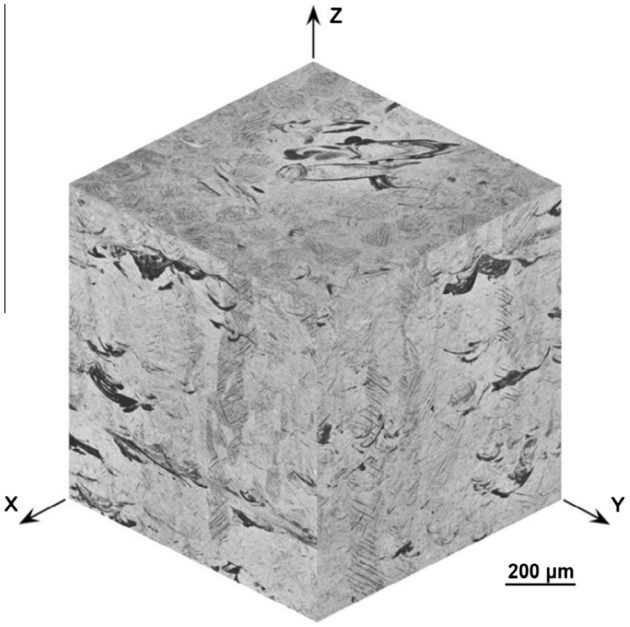

Fig. 8. Microstructure of DMLS Ti6Al4V (build direction parallel to *Z*-axis).

applied to the build to relieve, at least partially, the residual stresses that develop during material melting and solidification. Specimen surfaces were maintained in the as-fabricated state. Process qualification was carried out using tensile tests on specimens with machined surfaces that provided the following reference properties for the material, process and heat treatment: ultimate stress R_m = 1325 MPa, yield stress R_p = 1213 MPa, elongation to rupture $A\%$ = 4.5%.

3.2. Microstructural characterization

The 3-D etched microstructure of the present DMLS Ti6Al4V alloy, investigated with light microscopy [16], is shown in Fig. 8 where *Z* is the build direction.

The structure of Ti6Al4V is directional with a characteristic and similar texture in the *X–Z* and *Y–Z* cut planes, i.e. perpendicular to the raster laser tracks. Intersections of such tracks with the respective cutting plane show as a series of dark areas generated by the local intense laser energy distribution.

Fig. 9a shows the system of dark areas elongated in the *Y* direction in the *Y–Z* cut plane (analogously in the *X* direction of the *Z–X* cut plane) shows the layer-by-layer material generation process. Columnar grains of primary β-phase structure develop in the build direction (i.e. vertical direction in Fig. 9a). They grow epitaxially during the material processing and are much larger than the individual layer thickness (i.e. typically 30 µm). Fig. 9a shows columnar grains of a width of 200–300 µm and very long (>1 mm) i.e. involving many layers. This finding agrees with [6]. Martensitic needles are visible and disposed according to an herring bone pattern within the grains.

A different texture develops on the cut plane *X–Y* of Fig. 9b. The laser moves with a raster motion on this plane and melt locally a material volume by high-energy pulses. Rounded and fine grains (diameter of 100 µm) form upon solidification of the melt pools.

The presence of pores and defects due to the DMLS process was examined in [16] and it is relevant for the discussion of the following fatigue characterization. In general pores and defects were very small indicating optimized process parameters. However the magnified view of the *Y–Z* plane shown in Fig. 10, reveals small defects distributed parallel to the horizontal direction (i.e. trace of laser scanning plane) and elongated in the same direction. This structural feature suggests a potential negative role when the applied cyclic stress is in the vertical direction (i.e. *Z*-axis and therefore *Z–X* specimens) while their orientation may not affect *Y–Z* specimens and *X–Y* specimens because the applied stress is parallel to layers (i.e. planes of defects).

4. Results and discussion

This section begins with the experimental results that motivated the study, i.e. the degree of anisotropy of the fatigue behavior of DMLS Ti6Al4V. Having obtained such results with a new testing system and test method, a subsequent section will check the present data with literature data obtained with standard test configurations.

4.1. Anisotropic high cycle fatigue behavior

Inspection of the material structure shown in Fig. 8 along with the specimen orientation with respect to build, Fig. 7, clarifies that the direction of the applied bending stress with respect to the layer-by-layer material structure. Namely, stress direction in *Z–X* specimens is orthogonal to the material layers, the stress in *X–Y* specimens in the plane of the last solidified layers, while the stress direction in *Y–Z* specimens is parallel to the layers.

High-cycle fatigue test data for the three specimen orientations obtained by the present test method are shown in Fig. 11. First, the scatter in the data for the same configuration is rather low suggest-

Please cite this article in press as: Nicoletto G. Anisotropic high cycle fatigue behavior of Ti–6Al–4V obtained by powder bed laser fusion. Int J Fatigue (2016), http://dx.doi.org/10.1016/j.ijfatigue.2016.04.032

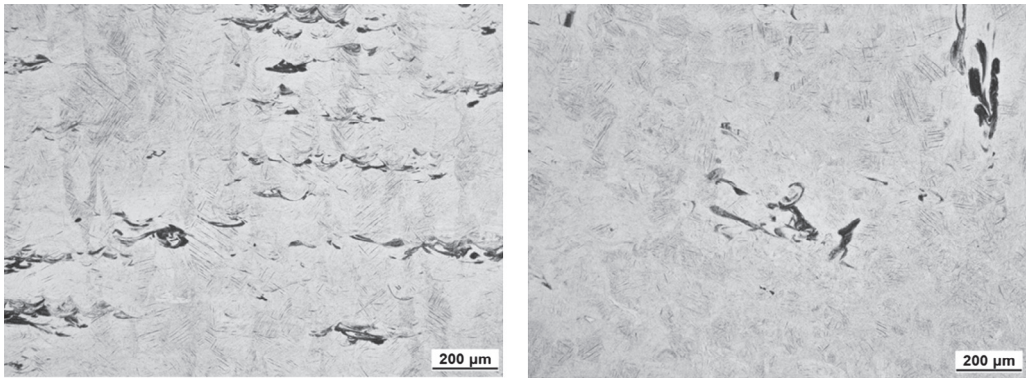

(a) elongated grains across multiple 30µm layers in Y-Z plane (Z axis is vertical)

(b) fine grain structure in X-Y plane due to meandering laser scan

Fig. 9. Microstructure of DMLS Ti6Al4V.

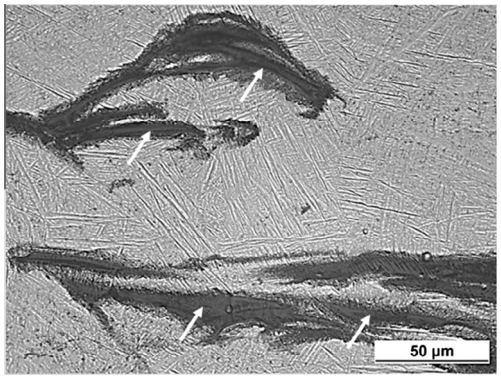

Fig. 10. Structural defects oriented perpendicular to build (*Z*-axis is vertical).

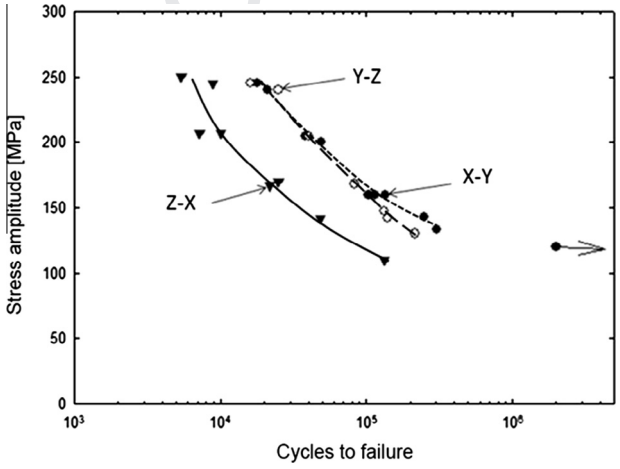

Fig. 11. Anisotropic fatigue behavior of stress relieved DMLS Ti6Al4V ($R = 0$).

ing that the small specimen size do not interact significantly with the material structure. The trend in a linear-log plot is well behaved with fatigue lives of the *Z–X* specimens that are considerably different and shorter than the other two specimen orientations. The presence of an anisotropic fatigue behavior of DMLS Ti–6Al–4V after a mild stress relieving treatment is therefore demonstrated and quantified.

Such novel data suggest a discussion of the role of stress orientation vs. build direction based on the microstructural features. The cyclic stress direction in the *Z–X* specimens is parallel to the build direction while in the *Y–Z* and *X–Y* specimens are perpendicular to build.

Therefore, the small interlayer defects shown in Fig. 10 apparently play a role in the fatigue damage process of the *Z–X* specimens and their fatigue life is significantly shorter than that of the two other specimen orientations.

Closer inspection of the plot demonstrates also that, although quite similar, the *Y–Z* specimen direction may be less performing than the *X–Y* specimen direction, especially at high number of cycles. A significant role on the fatigue behavior of *X–Y* and *Z–Y* specimens is played by the surface condition. The surface of the X–*Y* specimen is rather smooth (see top of Fig. 12a) with a fine grain structure shown in Fig. 9b. On the other hand, the surface of the *Y–Z* specimens is rougher than that of *X–Y* specimen (see top of Fig. 12b) because the layers intersect with the specimen surface where un-melted and semi-melted spheroidal particles of Ti6Al4V powder generate a porous layer of about 60 µm. The columnar grain structure of Fig. 9a may also negatively affect the fatigue behavior.

Therefore it may be concluded that the fatigue behavior of DMLS specimen oriented parallel to the build direction (i.e. *Z–X* specimens) are negatively affected by two contributing factors: i) interlayer defects unfavorably oriented with respect to applied stress and ii) rough surface finish, which is similar to that of *Y–Z* specimens (i.e. Fig. 12b).

It has to be stressed at this point that the present results of anisotropic fatigue behavior are related to a specific process and post fabrication stress relieving heat treatment. The influence of other post-fabrication heat treatments are currently investigated using the same experimental configuration.

4.2. Comparison with published data

The previous data, while well behaved and quantitative, have been obtained with a new specimen geometry and test methodology. Therefore, an assessment of the present fatigue data on DLMS Ti–6Al–4V with data from the literature is an important step toward the validation of the methodology. Unfortunately, the published information on the fatigue strength of DMLS Ti6Al4V alloy is limited and often fatigue data are obtained under different stress ratios *R* and loading conditions. Furthermore, specimen surfaces are polished to eliminate the inevitably negative impact of the as-processed surface, although it is most significant for the PBF application. Specimen dimensions may also introduce a size effect that is not readily quantified.

Please cite this article in press as: Nicoletto G. Anisotropic high cycle fatigue behavior of Ti–6Al–4V obtained by powder bed laser fusion. Int J Fatigue (2016), http://dx.doi.org/10.1016/j.ijfatigue.2016.04.032

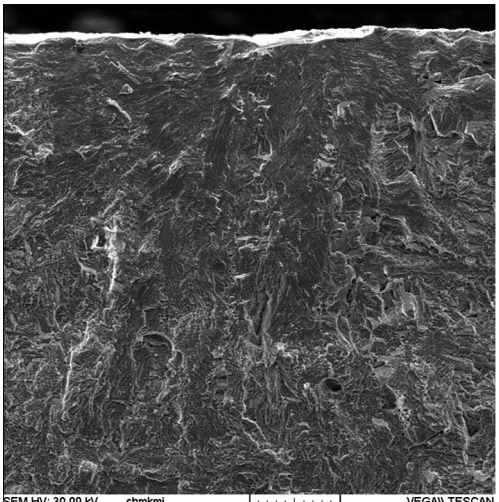

Fig. 12. Typical fatigue fracture surfaces showing the as-fabricated surface quality (top) of (a) *X*–*Y* specimens and (b) *Y*–*Z* specimens (fatigue cracks initiated at the top).

All these influencing factors can be qualitatively addressed using textbook knowledge of fatigue behavior in that: (i) an increase in specimen cross-section size is expected to lower the fatigue performance, (ii) a push–pull loading leads to more conservative fatigue data (shorter lives) than the bending loading condition, (iii) surface roughness decrease the fatigue performance [15].

As far as the mean stress effect (i.e. the role of the *R*-ratio on the results), several empirical models of varying complexity have been developed to quantify its role on fatigue strength. The simple Goodman relationship is used here to compute and compare fatigue data obtained under different *R* ratios in terms of an equivalent stress. Eq. (2) defines the equivalent stress σ_{eq} as

$$\sigma_{eq} = \frac{\sigma_a}{1 - \frac{\sigma_m}{R_m}} \quad (2)$$

where σ_a is the stress amplitude, σ_m is mean stress and R_m the ultimate strength of the material [15].

The present fatigue data obtained with the new test method are assessed in Fig. 13 using data from relevant studies of PBF Ti–6Al–4V and a common data representation in terms of equivalent stress σ_{eq} vs. number of cycles to failure [10–13]. The present best and worst fatigue data (i.e. *X*–*Y* and *Z*–*X* directions, respectively) are shown in Fig. 13 using black symbols and continuous trend lines.

Edwards and Ramulu [10], tested push–pull specimens produced Ti–6Al–4V by the SLM with an MTT 250 machine and tested in the as-produced condition. From the experimental point of view, the specimen cross-section was $8 \times 12\ mm^2$ and their fatigue stress ratio $R = -0.2$, therefore not too different from the present $R = 0$ condition. Furthermore they tested specimens oriented in the *Z* direction and two orthogonal directions in the *X*–*Y* plane so their applied stress directions were similar to that of the present *Y*–*Z* specimens. Their data and trend curves are plotted in Fig. 13 in magenta color and show that (i) the direction *Z* is associated to the lowest fatigue strength as in the present experiments, (ii) the combined effect of size, absence of stress relief, push–pull loading and presence of defects make them lower bounds of fatigue behavior of PBF Ti–6Al–4V alloy.

Van Hooreweder et al. [11], used an in-house SLM machine to fabricate push–pull specimens with minimum cross-section of $6 \times 3\ mm^2$. A stress relief treatment at 650 °C for four hours in a protective Argon atmosphere was performed on the specimens before testing. The fatigue behavior of the PBF material was determined using constant amplitude cyclic tensile loading ($R = 0$) at 75 Hz. In the finite fatigue region, seven smooth specimens were tested at different stress levels. In the infinite fatigue region (2×10^5–10^7 cycles) the staircase method, also known as the up-and-down method, was used to determine the endurance limit for the smooth specimens. Their fatigue data and trend lines are shown in Fig. 13 in green color. They commented that the fatigue resistance of SLM Ti–6Al–4V was substantially lower compared to the fatigue resistance of conventionally produced (wrought) specimens subjected to the same loading conditions. Their data are a little better than Edwards & Ramulu's direction *Z* data with which they share the type of loading, and differ in size and heat treatment [10].

Rekedal [12], recently reported an investigation using fatigue specimens fabricated using an EOSINT M 280 machine (i.e. DLMS process). Specimen cross section was $A = 3 \times 10 = 30\ mm^2$ and the loading condition was cyclic tension with $R = 0.1$. For budgetary reasons specimens were fabricated and tested only in the *x*-direction after removal of supports. The specimens underwent a stress relief heat treatment with exposure to 800 °C for 4 h in an Argon atmosphere as specified in the EOS Ti-64 Material Data

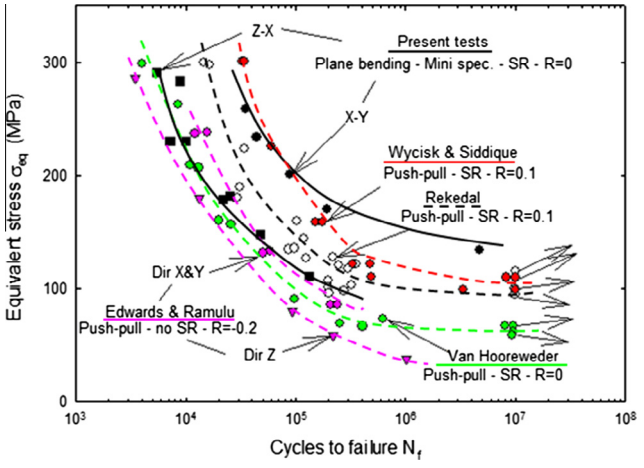

Fig. 13. Fatigue behavior of PBF Ti–6Al–4V using data from different sources.

Please cite this article in press as: Nicoletto G. Anisotropic high cycle fatigue behavior of Ti–6Al–4V obtained by powder bed laser fusion. Int J Fatigue (2016), http://dx.doi.org/10.1016/j.ijfatigue.2016.04.032

Sheet. Their data plotted in Fig. 13 with open symbols and black broken trend line, fall between the present *Z–X* (worst) and *X–Y* (best) directions. While their specimen orientation is similar to the *X–Y* direction, specimen size and type of loading possibly affect the data placing them close to present *Z–X* data.

Wycisk and Siddique [13], manufactured smooth 5-mm-diameter specimens (cross-section area $A = 20\ mm^2$) at 45° to the base plate using the EOS M270xt machine. To eliminate residual tensile stresses which are detrimental to fatigue performance, a stress-relieving heat treatment was performed at 650 °C for 3hrs in vacuum followed by cooling in Argon. Tests were performed with a stress ratio $R = 0.1$ at a frequency of 50 Hz. Their data plotted in Fig. 13 in red symbols and broken red trend line correlate well to those of Rekedal's at long lives and with the present *X–Y* data at short lives.

Fig. 13 represents an attempt of determining the fatigue performance of PBF Ti–6Al–4V using data from different sources and generated with specimens that differ in many ways and the stress ratio managed with Eq. (2). In general the known influences on fatigue behavior of the testing parameters are confirmed [15], namely: (i) push–pull loading is more severe on the material than cyclic bending, (ii) an increase in specimen size reduces the measured fatigue strength, (iii) the surface finishing increases the fatigue strength compared to as-fabricated condition.

On the other hand, the fatigue behavior of PBF Ti–6Al–4V is influenced by: (i) microstructure, because it introduces a directional effect; (ii) defects, that being typically located between adjacent layers, affect most the direction *Z*, (a HIP treatment often considered reduces that influence of defects but would lower the material strength [12]); (iii) post-fabrication heat treatment, which not only relieves residual stresses but should be selected to simultaneously optimize strength, ductility and fatigue behavior; (iv) surface finish, which is not always an option when recessed areas are present in the PBF part and when there are cost constrains.

The plot of Fig. 13 clearly demonstrates that the complex fatigue behavior of PBF Ti–6Al–4V. A comment may be contributed now as regards the fatigue performance of PBF Ti–6Al–4V in relation to wrought Ti–6Al–4V. First of all, the wrought alloy has been investigated extensively for its notable engineering importance in the last 30 years. Aspects such as heat treatments, surface finish, structural features and high vs. very high cycle fatigue behavior have been investigated using smooth specimens and reported in the literature. Although a review of that information is beyond the scope of the present work, the high cycle fatigue strength of this alloy in the wrought form is reported to range between 350 MPa and 700 MPa [15,17]. In all studies great care was devoted to specimen surface quality because of the sensitivity in fatigue. Since the data of Fig. 13 were all obtained using specimens with as-produced surfaces it is no surprise the fatigue strength of PBF Ti–6Al–4V is significantly lower that of the wrought material [15].

Nonetheless, only the clarification and understanding of the different affecting factors (internal and external) on the material behavior may lead to process optimization and full exploitation of PBF technology in the design and fabrication of durable, safe and cost competitive parts.

5. Conclusions

An original fatigue test methodology aimed at PBF materials was presented and directed to the evaluation of the anisotropic fatigue behavior of DMLS Ti6Al4V. The presence of such anisotropy is intrinsic to the specific and complex microstructure obtained by the layer-by-layer development of the part produced by DMLS.

The directionality of the high cycle fatigue behavior was confirmed and quantified. The sources of such behavior have been traced to the material structure and surface roughness.

Comparison of the present test results with data from literature demonstrates the efficiency and reasonable accuracy of the new specimen geometry and test method. The proposed testing method permits substantial resource saving (material, process time, etc.) that are especially welcome for developmental studies of PBF alloys and process parameters. Standard fatigue test methods for PBF materials are nonetheless required.

The comparison of fatigue data obtained with a variety of test methods and test parameters discussed here clarified the role of many intrinsic (material-dependent) and extrinsic (test-method-dependent) factors on the measured fatigue behavior of PBF Ti6Al4V.

Acknowledgments

The author acknowledges the scientific contributions of colleagues Prof. R. Konečna and Ing. A. Bača, University of Žilina, Slovakia, to the metallographic and fractographic characterizations and the specimen fabrication with the EOS system by BEAM-IT Srl, Fornovo (PR), Italy.

References

[1] Gibson I, Rosen D, Stucker B. Additive manufacturing technologies: rapid prototyping to direct digital manufacturing. New York: Springer; 2014. p. 498. ISBN 978-1-4939-2113-3.
[2] Gebhardt A. Understanding additive manufacturing. Munich: Hanser Publishers; 2011. p. 164. ISBN 978-3-446-43162-1.
[3] Meier H, Haberland C. Experimental studies on selective laser melting of metallic parts. Materialwiss Werkst 2008;39(9):665–70.
[4] Thijs L, Verhaeghe F, Craeghs T, Van Humbeeck J, Kruth JP. A study of the microstructural evolution during selective laser melting of Ti–6Al–4V. Acta Mater 2010;58:3303–12.
[5] Kruth JP, Levy G, Klocke F, Childs THC. Consolidation phenomena in laser and powder-bed based layered manufacturing. CIRP Ann – Manuf Technol 2007;56:730–59.
[6] Qiu C, Adkins NJE, Attallah MM. Microstructure and tensile properties of selectively laser-melted and of HIPed laser-melted Ti–6Al–4V. Mater Sci Eng 2013;A578:230–9.
[7] Vilaro T, Colin C, Bartout JD. As-fabricated and heat-treated microstructures of the Ti–6Al–4V alloy processed by selective laser melting. Metall Mater Trans A 2011;42A:3190–9.
[8] Simonelli M, Tse Y, Tuck C. Effect of the build orientation on the mechanical properties and fracture modes of SLM Ti–6Al–4V. Mater Sci Eng 2014;616:1–11.
[9] Mercelis P, Kruth JP. Residual stresses in selective laser sintering and selective laser melting. Rapid Prototyping J 2006;12:254–65.
[10] Edwards P, Ramulu M. Fatigue performance evaluation of selective laser melted Ti–6Al–4V. Mater Sci Eng: A 2014;598:327–37.
[11] Van Hooreweder B et al. On the determination of fatigue properties of Ti6Al4V produced by selective laser melting. In: Proc 53rd AIAA/ASME/ASCE/AHS/ASC structures, structural dynamics and materials conference, Honolulu, Hawaii. http://dx.doi.org/10.2514/6.2012-1733.
[12] Rekedal KD. Investigation of the high-cycle fatigue life of selective laser melted and hot-isostatically-pressed Ti–6Al–4V. M.S. Thesis, AFIT-ENY-MS-15-M-212 Wright-Patterson AFB, Ohio; 2015.
[13] Wycisk E, Emmelmann C, Siddique S, Walther F. High cycle fatigue (HCF) performance of Ti–6Al–4V alloy processed by selective laser melting. Adv Mater Res 2013;816–817:134–9.
[14] Nicoletto G et al. Tensile and fatigue behavior of Ti6Al4V produced by selective laser melting. In: Proc 4th international conference of engineering against failure (ICEAF IV), Skiathos, Greece; 2015.
[15] Nicholas T. High cycle fatigue: a mechanics of materials perspective. San Diego (CA): Elsevier; 2006.
[16] Konečná R et al. Microstructure, defects and fractography of Ti6Al4V alloy produced by SLM and DMLS. Powder Metall Prog 2015;15:86–93.
[17] Wagner L, Bigoney JK. Fatigue of titanium alloys. In: Peters M, Leyens C, editors. Titanium and titanium alloys fundamentals and applications. Wiley VCH; 2003. p. 153–82.